Geochemistry, Geophysics, Geosystems®

RESEARCH ARTICLE
10.1029/2021GC010249

Key Points:

- Unidirectional precipitation of $BaCO_3$ in HCO_3^--dominated solutions leads to more negative carbon, oxygen, and clumped isotope values
- Kinetic fractionation factors of oxygen and clumped isotopes between HCO_3^- and $BaCO_3$ are correlated and temperature dependent
- Isotopic analyses reveal a significant preferential incorporation for CO_3^{2-} over HCO_3^- during rapid carbonate growth

Correspondence to:
W. Deng,
wfdeng@gig.ac.cn

Citation:
Guo, Y., Deng, W., & Wei, G. (2022). Experimental constraints on clumped isotope fractionation during $BaCO_3$ precipitation. *Geochemistry, Geophysics, Geosystems*, *23*, e2021GC010249. https://doi.org/10.1029/2021GC010249

Received 5 NOV 2021
Accepted 8 MAR 2022

Experimental Constraints on Clumped Isotope Fractionation During $BaCO_3$ Precipitation

Yangrui Guo[1,2], Wenfeng Deng[1,2], and Gangjian Wei[1,2]

[1]State Key Laboratory of Isotope Geochemistry, CAS Center for Excellence in Deep Earth Science, Guangzhou Institute of Geochemistry, Chinese Academy of Sciences, Guangzhou, China, [2]Southern Marine Science and Engineering Guangdong Laboratory (Guangzhou), Guangzhou, China

Abstract Reliable temperature reconstruction by carbonate clumped isotope (Δ_{47}) thermometry requires isotopic equilibrium during carbonate growth. However, many carbonate minerals grow at high rates and exhibit disequilibrium isotopic states. Carbonate Δ_{47} disequilibrium arising from kinetic isotope effects (KIEs) specific to carbonate growth still remains unclear, and requires experimental constraints. Here we present a series of rapid witherite ($BaCO_3$) precipitation experiments intended to constrain bulk carbon, oxygen and clumped isotopic fractionation during unidirectional precipitation of $BaCO_3$ from dissolved inorganic carbon solutions under various pH and temperature conditions. We found that rapid $BaCO_3$ growth can lead to lower $\delta^{13}C$, $\delta^{18}O$, and Δ_{47} values in HCO_3^--dominated solutions, especially at low temperatures. Our experiments provide constraints on kinetic fractionation factors (KFFs) associated with the rapid carbonate growth and their temperature dependence. KFFs for $\delta^{13}C$ and $\delta^{18}O$ are broadly consistent with previous experimental estimates, although the Δ_{47} KFF for $BaCO_3$ precipitation from HCO_3^--dominated solution is not consistent with an earlier theoretical estimate, necessitating a re-evaluation of the current model of the KIE associated with carbonate growth. Our results clearly verify a preference for the CO_3^{2-} pathway during carbonate precipitation, with important implications for new isotope fractionation models for natural carbonates. The fractionation relationship between Δ_{47} and $\delta^{18}O$ found in this study allows more precise identification of KIEs associated with rapid carbonate growth.

1. Introduction

Carbonate clumped isotope (Δ_{47}) thermometry is based on the temperature-dependent bonding of ^{13}C and ^{18}O within the lattice of carbonate minerals relative to that expected when all isotopes are randomly distributed (Ghosh et al., 2006; Schauble et al., 2006). The clumped isotope geochemistry of carbonates provides a single-phase geothermometer independent of the stable isotopic composition of the parent fluid, and is a frontier in the development of paleo-temperature proxies (Eiler, 2007, 2011). The last decade has seen an increasing use of clumped isotopes in studies of climate change on various geological time scales (Dennis et al., 2013; Fernandez et al., 2021; Finnegan et al., 2011; Leutert et al., 2020; Petersen et al., 2016; Vickers et al., 2020). Accurate estimation of paleo-temperatures requires clumped isotopes to be in equilibrium during carbonate precipitation, but many natural carbonates present disequilibrium Δ_{47} values, as in oxygen isotope thermometry (Daëron et al., 2019; Ghosh et al., 2006; Watkins & Hunt, 2015). An understanding of causes of Δ_{47} disequilibrium in carbonates is therefore required for reliable application of clumped isotope thermometry.

Key reactions such as CO_2 hydration/hydroxylation and HCO_3^- dehydration/dehydroxylation exert important kinetic isotope effects (KIEs) on Δ_{47} values of the dissolved inorganic carbon (DIC) and thus of precipitated carbonates, with recent studies of causes and controls of Δ_{47} disequilibrium in carbonates focusing mainly on the DIC–H_2O–CO_2 system (Affek & Zaarur, 2014; Daëron et al., 2011; Guo, 2020; Guo & Zhou, 2019; Staudigel & Swart, 2018; Uchikawa et al., 2021). When isotopic exchange between DIC species and H_2O or the ordering state of ^{13}C–^{18}O bonds within the DIC species are at equilibrium, rapidly grown carbonates may inherit the Δ_{47} values of DIC species, that is, the weighted sum of their distinct equilibrated Δ_{47} values, if all DIC species are quantitatively precipitated (Hill et al., 2014; McCrea, 1950; Tripati et al., 2015). The relative abundances of DIC species are controlled mainly by pH (Zeebe & Wolf-Gladrow, 2001). Carbonates growing at different fluid pH levels thus likely exhibit different Δ_{47} values, which may be responsible for Δ_{47} disequilibrium in biogenic carbonates, such as certain species of deep-sea corals (Saenger et al., 2017; Spooner et al., 2016). A comprehensive exploration of the mechanism of Δ_{47} disequilibrium thus requires consideration of both DIC–H_2O–CO_2 and $CaCO_3$–DIC

systems, with a better understanding of KIEs between carbonate and precipitating DIC species required for the latter to elucidate isotopic fractionation during carbonate growth.

The KIE generally refers to the change of the reaction rate in a given chemical reaction when isotopic substitution is involved (Zeebe & Wolf-Gladrow, 2001). The change of the reaction rate means that light and heavy isotopologues react at different rates, resulting in a characteristic difference in isotope composition between the reactant and the reaction product (Sade et al., 2020). For example, a calcium carbonate precipitation reaction may be described in two forms in terms of carbon isotopes (^{12}C and ^{13}C):

$$Ca^{2+} + {}^{12}CO_3^{2-} \underset{{}^{12}k_-}{\overset{{}^{12}k_+}{\rightleftarrows}} Ca^{12}CO_3 \quad (1)$$

$$Ca^{2+} + {}^{13}CO_3^{2-} \underset{{}^{13}k_-}{\overset{{}^{13}k_+}{\rightleftarrows}} Ca^{13}CO_3 \quad (2)$$

Because of the KIE involved during the $CaCO_3$ growth, the reaction rate constant ($^{12}k+$) for the light isotope (^{12}C) is usually larger than that ($^{13}k+$) for the heavy isotope (^{13}C), leading to depletion in ^{13}C content in the reaction product $CaCO_3$ with respect to CO_3^{2-}. The magnitude of the KIE for the forward reaction ($CaCO_3$ growth) is defined by a kinetic fractionation factor (KFF), which equals the ratio of the rate constants ($^{12}k+/^{13}k+$; Zeebe & Wolf-Gladrow, 2001). The difference in carbon isotope composition ($\delta^{13}C$) between the reactant and the reaction product is determined by KIEs associated with reaction rate constants both in forward and reverse reactions (i.e., $CaCO_3$ precipitation and dissolution, respectively). If no significant reverse reaction occurs or the $CaCO_3$ grows so rapid that the whole reaction is unidirectional, the KIE associated with rapid $CaCO_3$ growth is fully expressed and its KFF can be determined directly by the difference in $\delta^{13}C$ values between $CaCO_3$ and CO_3^{2-} (Sade et al., 2020).

Exploring the Δ_{47} KIEs specific to carbonate growth was first attempted by Daëron et al. (2011) based on three synthetic stalagmites with different growth rates. However, the corresponding Δ_{47} fractionation signatures they observed were not controlled independently by carbonate growth as the CO_2 degassing effect was also involved. Watkins and Hunt (2015) applied the ion-by-ion calcite growth model of Wolthers et al. (2012) to describe KIEs arising from the mass-dependent transport of HCO_3^- or CO_3^{2-} from bulk solution to the mineral growth surface. A series of calcites precipitated from isotopically equilibrated DIC solutions at different pH values has been used to constrain KFFs for oxygen isotopes, but not for clumped isotopes (Watkins et al., 2013, 2014), suggesting that the ion-by-ion model could also be verified on the basis of KFFs. This requires determination of Δ_{47} values of calcites precipitated at different pH levels from isotopically equilibrated DIC solutions, with isotopic disequilibrium arising from the DIC–H_2O system minimized by the enzyme carbonic anhydrase (CA) in previous studies (Watkins et al., 2013, 2014). However, this approach may be challenging when constraining the KFF between carbonates and CO_3^{2-} as the DIC isotopic equilibration at room temperature (~25°C) is very slow at pH > 12, even in the presence of CA (Tripati et al., 2015; Uchikawa & Zeebe, 2013).

Rapid precipitation of witherite ($BaCO_3$) is experimentally achievable, with an assumed unidirectional reaction and no significant reverse reaction to DIC species through dissolution (Beck et al., 2005; Kim et al., 2006; Sade et al., 2020). It should therefore be possible to determine Δ_{47} KFFs during carbonate growth by applying the $BaCO_3$ precipitation method, as often done in investigations of oxygen isotopic fractionation in the carbonate system (Beck et al., 2005; Kim & O'Neil, 1997; Kim et al., 2006; Sade et al., 2020; Staudigel & Swart, 2018; Uchikawa & Zeebe, 2012, 2013; Yumol et al., 2020). However, caution should be taken in applying the KFFs to other carbonates, as the precipitation-specific KFFs for $BaCO_3$ might differ from those for calcite, dolomite, or other carbonates of interest.

In this study, a series of $BaCO_3$ precipitation experiments were performed at temperature and pH ranges of 15–60°C and 8.3–11.5, respectively. $BaCO_3$ was fractionally precipitated from a quasi-infinite DIC reservoir with only ~0.5% in mole fraction of the DIC being precipitated within 10 min. The carbon, oxygen, and clumped isotopic compositions of the $BaCO_3$ were compared with those of $BaCO_3$ immediately and quantitatively precipitated from the same reservoir to constrain the KFFs during mineral growth. We deem that the growth of $BaCO_3$ in such short time can avoid the isotopic re-equilibration through dissolution of $BaCO_3$ and there was no need to consider the isotopic composition or equilibrium state of the DIC solution. This study quantitatively constrains

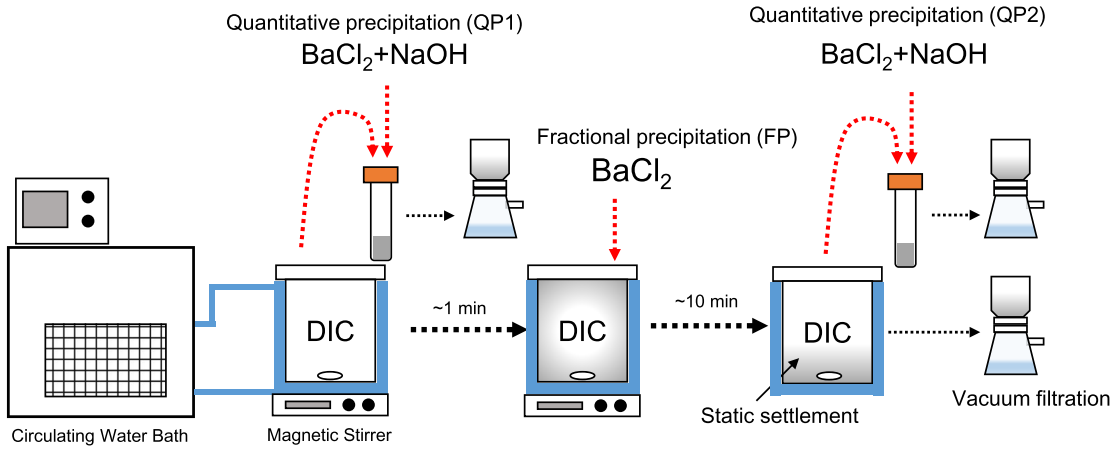

Figure 1. Schematic diagram of the experimental setup used in this study. The temperature of each $BaCO_3$ precipitation was maintained by a circulating water bath. Each experiment under specific pH and temperature conditions involved two quantitative precipitations and one fractional precipitation of $BaCO_3$ crystals from the same dissolved inorganic carbon solution.

the clumped isotope fractionation effect associated with rapid $BaCO_3$ precipitation and its dependence on pH and temperature, which have not been confirmed in previous studies.

2. Methods

2.1. $BaCO_3$ Precipitation Experiments

A series of $BaCO_3$ precipitation experiments based on the methods of Kim et al. (2006) and Sade et al. (2020) were performed as depicted in Figure 1. DIC solutions (0.06 M) were prepared by dissolving ~5 g reagent grade $NaHCO_3$ (with $\delta^{13}C$ and $\delta^{18}O$ values of −15.26‰ and −17.46‰, respectively, relative to the Vienna Pee Bee Belemnite [VPDB]) in separate flasks containing 1 L deionized water, and used under different conditions as described in Table 1. NaOH (4 M) and HCl (4 M) solutions were used to adjust pH and DIC speciation. A pH meter (San-Xin Instrumentation Inc., SX800 model, Shanghai, China) was used with calibration by standard pH buffers. Reaction flasks were held at 15, 25, 40, or 60°C (±0.05°C) in water baths with constant magnetic stirring. Solutions were equilibrated for >24 hr without necessarily reaching isotopic equilibrium. For quantitative DIC precipitation (QP1), a small volume (5 mL) of DIC solution was aspirated using a syringe and was then injected into a headspace vial (pre-purged with high purity nitrogen) containing excess $BaCl_2$ (1 mL, 1 M) and NaOH (1 mL, 1 M) solutions, such that all DIC species (mainly HCO_3^- and CO_3^{2-} species) precipitated instantaneously as $BaCO_3$ minerals without significant atmospheric contact (Beck et al., 2005). This step was followed immediately by injection of 1 mL $BaCl_2$ solution (0.3 M) into the reaction flask to precipitate fractional (~0.5% in mole fraction) DIC species, referred to here as fractional precipitation (FP). This was repeated for all experiments, except for that at 15°C and pH 8.55 where 0.2 mL saturated $BaCl_2$ solution was used to increase the nucleation rate of $BaCO_3$ crystals. These reagent concentrations provided sufficient (>50 mg) $BaCO_3$ for isotopic analysis, and minimized isotopic fractionation due to Rayleigh distillation effects during removal of DIC species by $BaCO_3$ precipitation (Kim et al., 2006). The FP experiments were ca. 10 min in duration, including ca. 2 min for precipitation with magnetic stirring and ca. 8 min for static settlement of $BaCO_3$. The first crystals of $BaCO_3$ usually occurred within ca. 30 sec. A further 5 mL of the DIC solution was aspirated from the liquid surface for another quantitative DIC precipitation (QP2). The difference in isotopic compositions of $BaCO_3$ between the QP1 and QP2 experiments allows us to evaluate the variation of the isotopic composition of the DIC solution during precipitation experiments. $BaCO_3$ precipitates from QP1, FP, and QP2 were vacuum filtered through a 0.45 μm cellulose acetate membrane immediately after precipitation. The filters were rinsed several times with deionized water, dried at 50°C for at least 24 hr, and stored in vials for later isotopic analysis.

Table 1
Experimental Conditions and Isotope Data for Quantitative and Fractional Experiments

Sample ID	Precipitation method	Temp. (°C)	pH	Total [DIC] (mmol/L)	Yield (mg)	$[HCO_3^-]$/[DIC] (%)	$[CO_3^{2-}]$/[DIC] (%)	$\delta^{13}C$ (VPDB ‰)	1 SD[a]	$\delta^{18}O$ (VPDB ‰)	1 SD[a]	$\Delta_{47\text{-CDES90}}$ (‰)	1 SD[a]	*n*
BPL15R-1	QP1	15	8.55	60	61.1	98.0	1.3	−15.26	0.00	−2.64	0.02	0.672	0.014	2
BPL15R-K	FP	15	8.55	60	104.8	98.0	1.3	−16.60	0.00	−7.90	0.05	0.619	0.003	2
BPL15R-2	QP2	15	8.55	60	59.2	98.0	1.3	−15.13	0.03	−2.50	0.04	0.681	0.002	2
BPH15-1	QP1	15	11.43	60	58.4	9.1	90.9	−15.11	0.09	−3.55	0.07	0.660	0.017	3
BPH15-K	FP	15	11.43	60	63.1	9.1	90.9	−15.13	0.18	−5.57	0.08	0.655	0.017	2
BPH15-2	QP2	15	11.43	60	58.8	9.1	90.9	−15.00	0.23	−3.84	0.09	0.659	0.002	2
BPL25R-1	QP1	25	8.63	60	57.0	97.5	1.9	−14.91	0.16	−4.41	0.09	0.637	0.020	3
BPL25R-K	FP	25	8.63	60	54.2	97.5	1.9	−16.40	0.02	−9.35	0.04	0.580	0.013	2
BPL25R-2	QP2	25	8.63	60	55.1	97.5	1.9	−15.03	0.03	−4.32	0.04	0.630	0.005	2
BPMR25-1	QP1	25	9.78	60	59.0	78.0	22.0	−15.27	0.06	−4.63	0.06	0.649	0.008	2
BPMR25-K	FP	25	9.78	60	58.5	78.0	22.0	−15.72	0.10	−8.05	0.07	0.613	0.007	2
BPMR25-2	QP2	25	9.78	60	57.7	78.0	22.0	−15.27	0.05	−4.55	0.02	0.637	0.004	2
BPM25-1	QP1	25	10.45	60	57.8	43.1	56.9	−15.17	0.03	−17.39	0.04	0.500	0.005	2
BPM25-K	FP	25	10.45	60	58.5	43.1	56.9	−15.24	0.01	−18.71	0.03	0.499	0.011	2
BPM25-2	QP2	25	10.45	60	59.0	43.1	56.9	−15.28	0.00	−17.42	0.06	0.487	0.000	2
BPH25-1	QP1	25	11.45	60	58.0	7.0	93.0	−15.11	0.06	−13.21	0.04	0.527	0.002	2
BPH25-K	FP	25	11.45	60	58.4	7.0	93.0	−15.07	0.03	−13.24	0.08	0.533	0.022	3
BPH25-2	QP2	25	11.45	60	58.1	7.0	93.0	−15.33	0.02	−13.17	0.01	0.538	0.012	2
BPL40-1	QP1	40	8.38	60	59.5	97.8	1.4	−15.25	0.18	−7.28	0.04	0.597	0.017	2
BPL40-K	FP	40	8.38	60	53.8	97.8	1.4	−16.51	0.01	−11.93	0.04	0.546	0.005	2
BPL40-2	QP2	40	8.38	60	59.5	97.8	1.4	−15.21	0.05	−7.14	0.02	0.588	0.016	3
BPH40-1	QP1	40	11.41	60	54.0	6.1	93.9	−15.22	0.03	−7.19	0.10	0.609	0.025	3
BPH40-K	FP	40	11.41	60	59.5	6.1	93.9	−15.11	0.02	−7.04	0.12	0.592	0.008	2
BPH40-2	QP2	40	11.41	60	59.3	6.1	93.9	−15.18	0.05	−7.24	0.02	0.604	0.020	2
BPL60-1	QP1	60	8.30	60	59.1	97.6	1.4	−15.39	0.06	−10.06	0.03	0.546	0.016	3
BPL60-K	FP	60	8.30	60	54.3	97.6	1.4	−16.00	0.01	−14.31	0.03	0.518	0.002	2
BPL60-2	QP2	60	8.30	60	57.9	97.6	1.4	−15.44	0.04	−10.15	0.01	0.548	0.013	3
BPH60-1	QP1	60	11.28	60	60.1	6.7	93.3	−15.55	0.04	−10.95	0.01	0.559	0.004	2
BPH60-K	FP	60	11.28	60	57.8	6.7	93.3	−15.26	0.01	−10.93	0.01	0.560	0.004	2
BPH60-2	QP2	60	11.28	60	59.7	6.7	93.3	−15.40	0.06	−10.91	0.01	0.550	0.010	2

[a]1 SD refers to 1 standard deviation based on replicates.

2.2. Isotopic Analyses

Bulk carbon, oxygen, and clumped isotopic analyses were performed at the State Key Laboratory of Isotope Geochemistry, Guangzhou Institute of Geochemistry, Chinese Academy of Sciences, Guangzhou, with a dual-inlet isotope ratio mass spectrometer (IRMS; 253 Plus, ThermoFisher Scientific™, USA), following analytical procedures described previously by Guo et al. (2019). Briefly, carbonate (5–8 mg) was digested in H_3PO_4 (ρ = ~1.94 g/cm^3) at 90°C to produce CO_2 gases, which was collected cryogenically and purified by passage through two cold traps (ethanol slush at −90°C) and an adsorbent trap (PoraPak Q at −20°C, without using carrier gas) before IRMS analysis. The instrument was configured to simultaneously measure *m*/*z* 44–49 with a signal intensity of 15 V at *m*/*z* 44 and an *m*/*z* 47.5 cup for background correction. Each measurement comprised 60 sample/standard cycles, with 20 s integration per cycle. Each sample was analyzed at least twice, repeating acid digestion, gas purification, and instrument analysis with separate aliquots of each $BaCO_3$ sample. The reference

CO_2 gas had $\delta^{13}C$ and $\delta^{18}O$ values of −26.78‰ and −8.86‰, respectively. Its bulk isotopic compositions were normalized to two IAEA standards (NBS19 and NBS18) and are reported in VPDB scale. Bulk isotopic compositions and raw Δ_{47} values of measured gases are obtained relative to that of the reference working gas, calculated using the Easotope software (John & Bowen, 2016) and processed with the International Union of Pure and Applied Chemistry recommended parameters for ^{17}O correction (Brand et al., 2010; Daëron et al., 2016; Petersen et al., 2019). To correct for the dependence of Δ_{47} on δ_{47} values due to an inherent linearity issue with the IRMS, a set of CO_2 gases with δ_{47} values of −14‰ to +32‰ was analyzed after heating to 1000°C for ∼2 hr to obtain internal isotopologue equilibrium (Huntington et al., 2009). To allow reporting the Δ_{47} data on the Carbon Dioxide Equilibrium Scale at 90°C acid-digestion temperature (CDES90), several equilibrated CO_2 gases prepared by CO_2–H_2O exchange reaction at 25°C (Dennis et al., 2011) were analyzed.

Carbonate standards (C1 and BACS; Guo et al., 2019) were analyzed together with $BaCO_3$ samples to monitor instrument drift. The resulting mean $\Delta_{47\text{-CDES90}}$ values of these two standards were 0.318‰ (1SD = 0.014‰, n = 10) and 0.648‰ (1SD = 0.016‰, n = 11) for the C1 and BACS, respectively. These values agree with the results of a recent study in the same lab (Guo et al., 2021) if not applying the acid fractionation factor (AFF) of 0.088‰ (Petersen et al., 2019). The mean $\Delta_{47\text{-CDES90}}$ value of C1 (0.318 ± 0.014‰) is also similar to the community-derived consensus Δ_{47} value of 0.302‰ reported from Bernasconi et al. (2021), which was normalized on the Intercarb-Carbon Dioxide Equilibrium Scale (I-CDES) based on a series of ETH standards. As no ETH standards were measured in this study, we are unable to directly normalize the $\Delta_{47\text{-CDES90}}$ data to the I-CDES scale. However, as ETH standards were measured along with the BACS and C1 during a different measurement session in our lab (Guo et al., 2021) and the mean $\Delta_{47\text{-CDES90}}$ values of these ETH standards (0.222 ± 0.013‰, 0.622 ± 0.017‰, and 0.444 ± 0.015‰, for ETH-1, ETH-3, and ETH-4, respectively) were similar to the multi-laboratory determined $\Delta_{47\text{-CDES90}}$ values (0.205‰, 0.613‰, and 0.450‰, for ETH-1, ETH-3, and ETH-4, respectively) reported in Bernasconi et al. (2021), the $\Delta_{47\text{-CDES90}}$ values of standards and samples determined in this study are essentially comparable to the values normalized to the I-CDES scale. This study aims to explore the difference of $\Delta_{47\text{-CDES90}}$ values obtained from different $BaCO_3$ precipitation experiments, which should be not affected by the choice of data normalization scheme. The AFF of Kim et al. (2007) was applied to correct ^{18}O fractionation during carbonate acid digestion assuming that witherite and calcite have similar AFF values, as reported earlier (Uchikawa & Zeebe, 2013). All raw isotopic data for $BaCO_3$ samples, carbonate standards, and gas standards are available on Zenodo (Guo, 2021).

2.3. Kinetic Isotope Fractionation Between DIC Species and $BaCO_3$

With no significant Rayleigh distillation effects during the quantitative and fractional precipitations (Section 3), KFF values for the two phases may be expressed as:

$$\Delta\delta^{13}C_{BaCO_3-DIC} \cong \delta^{13}C_{FP} - \delta^{13}C_{QP} \quad (3)$$

$$\Delta\delta^{18}O_{BaCO_3-DIC} \cong \delta^{18}O_{FP} - \delta^{18}O_{QP} \quad (4)$$

$$\Delta\Delta_{47\,BaCO_3-DIC} \cong \Delta_{47\,FP} - \Delta_{47\,QP} \quad (5)$$

where the subscript "$BaCO_3$ − DIC" refers to isotopic composition difference between the two phases ($BaCO_3$ crystal and DIC species), and is also related to the instantaneous precipitation of $BaCO_3$ from DIC solution without isotopic re-equilibration by $BaCO_3$ dissolution, and "QP" and "FP" represent quantitative and fractional precipitations, respectively. These KFFs describe the net result of isotopic partitioning for all unidirectional reactions associated with $BaCO_3$ formation. When determining the KFF between a single DIC species (HCO_3^- or CO_3^{2-}) and $BaCO_3$, we assigned solutions of pH 8.30–8.63 with $[HCO_3^-]$/[DIC] values of 97.5–98.0% as being dominated by HCO_3^- and those pH 11.28–11.45 with $[CO_3^{2-}]$/[DIC] values of 90.9–93.9% by CO_3^{2-}, respectively. DIC speciation in the experimental solutions was determined by the CO2sys program (Lewis & Wallace, 2006) with pH, temperature, and DIC concentration as input variables, and with the carbonic acid dissociation constants of Millero (1979) and the NBS pH scale.

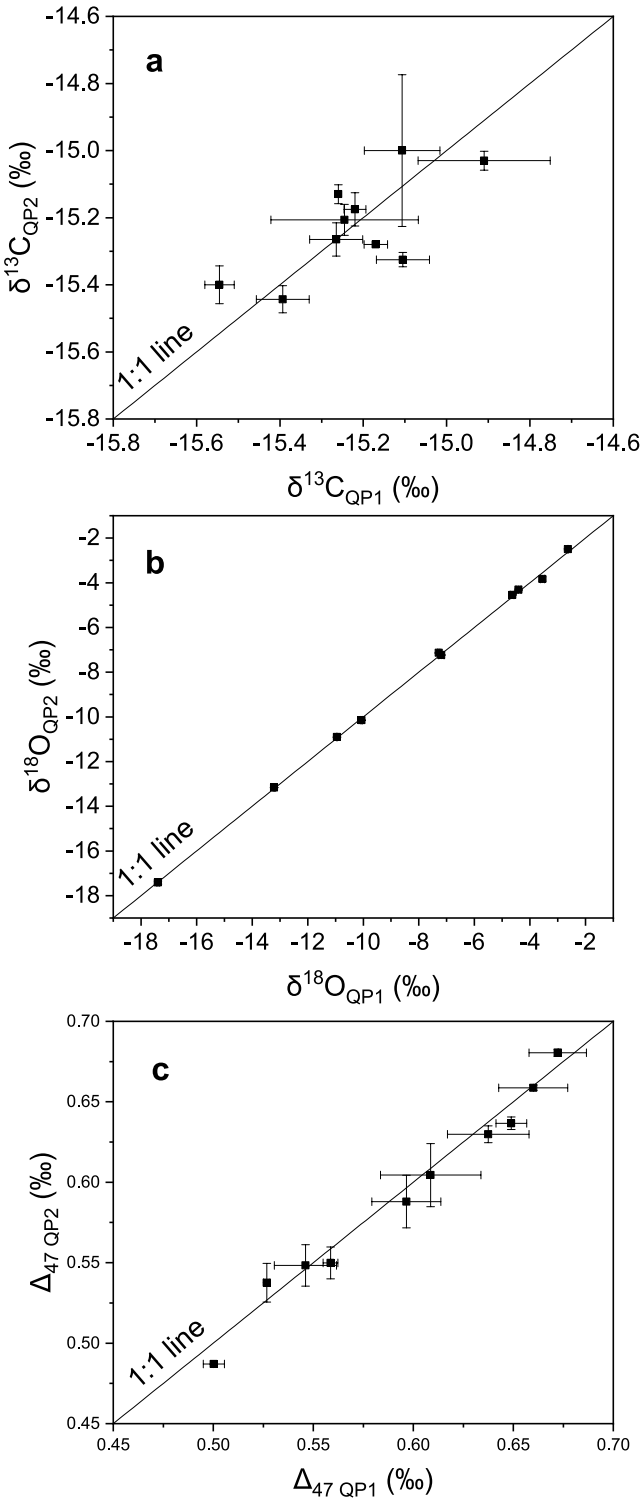

Figure 2. Comparison of isotopic data between the two quantitative precipitations (QP1 and QP2) of each experiment for (a) carbon, (b) oxygen, and (c) clumped isotopes. The error bars represent 2 SD errors from repeated isotope analyses in each experiment. The error bars on oxygen isotopes are smaller than symbols.

3. Results

Isotopic compositions ($\delta^{13}C$, $\delta^{18}O$, and Δ_{47}) of $BaCO_3$ samples formed in the QP1, FP, and QP2 experiments at all temperatures and pH values are provided in Table 1. Apart from sample BPL15R-K, where a large amount of $BaCl_2$ was added to the DIC solution, the measured mass of $BaCO_3$ for all experiments averaged 58.2 ± 2.1 mg (n = 29), broadly comparable with stoichiometric estimates based on DIC or $BaCl_2$ concentrations, suggesting a recovery rate of ~100%.

The range of $BaCO_3$ $\delta^{13}C$ values from the QP experiments (−15.5‰ to −15.0‰; Figure 2) is greater than typical analytical precision (~0.1‰) in carbonate $\delta^{13}C$ analyses. As all DIC solutions in QP experiments were prepared by the same $NaHCO_3$ reagent, the $BaCO_3$ $\delta^{13}C$ values should be the same value within error assuming that the $NaHCO_3$ powder is homogenous. Therefore, the scattered $BaCO_3$ $\delta^{13}C$ values may be attributed to contamination of other carbon source with $\delta^{13}C$ value different to that of the $NaHCO_3$ reagent or the possibility that the DIC solutions experienced various degree of CO_2 degassing among different experiments. A possible interference may be related to atmospheric CO_2 as a small amount of atmospheric CO_2 could be hydrated into the solution.

$BaCO_3$ $\delta^{18}O$ and Δ_{47} values from these QP experiments exhibited significant variations ranging from −18.71‰ to −2.64‰ and 0.487‰–0.660‰ for $\delta^{18}O$ and Δ_{47}, respectively (Table 1; Figure 2). These isotopic variations were presumably associated with equilibration of ^{18}O and ^{13}C–^{18}O bonds in DIC solution through hydration/dehydration and hydroxylation/dehydroxylation reactions. The state of isotopic equilibration in DIC solution is determined by the initial isotopic value (assigned by the $NaHCO_3$ reagent), the final equilibrium state, and the rate of equilibration of ^{18}O-associated and ^{13}C–^{18}O bonds, which is controlled mainly by temperature and pH (Beck et al., 2005; Staudigel & Swart, 2018; Uchikawa et al., 2021). As the QP experiments were carried out at various temperatures and pH conditions (Table 1), it is reasonable to expect a large range in $\delta^{18}O$ and Δ_{47} values in $BaCO_3$ precipitated from the DIC solution. It should be noted that whether or not the DIC solution was at isotopic equilibrium in each QP experiment is not important, as we mainly focus on KFFs between DIC species and $BaCO_3$ during precipitation. It is therefore essential to make sure that both the FP and QP experiments were done at the same temperature, pH, and isotopic composition of DIC solution. The isotopic compositions of $BaCO_3$ from the QP1 and QP2 experiments were generally similar within error (Figure 2), suggesting that the isotopic compositions of DIC solution remained unchanged after the FP. This means that the variation of $\delta^{13}C$ values due to interferences from other carbon sources and CO_2 degassing, and the variations of $\delta^{18}O$ and Δ_{47} values related to DIC isotopic equilibration were negligible during the time gap (~11 min) between the two QP experiments (QP1 and QP2). In this case, the significant variations of isotopic compositions in $BaCO_3$ observed here did not affect the determination of KFFs at specific pH and temperature because they were removed through Equations 3–5. For the same reason, the Rayleigh distillation effect on isotopic compositions associated with the removal of DIC portions (~0.5% in mole fraction) from the whole solution during FP experiment can be neglected as well.

KFFs specific to experimental conditions were determined using Equations 3–5 and by assigning isotopic compositions of quantitative precipitation as average values of the QP1 and QP2 experiments (Table 2). The

Table 2
Kinetic Fractionation Factors Specific to Different Experimental Conditions

Temp. (°C)	pH	$\Delta\delta^{13}C_{BaCO_3-DIC}$ (‰)	1 SD[a]	$\Delta\delta^{18}O_{BaCO_3-DIC}$ (‰)	1 SD[a]	$\Delta\Delta_{47\,BaCO_3-DIC}$ (‰)	1 SD[a]
15	8.55	−1.41	0.03	−5.33	0.06	−0.057	0.015
15	11.43	−0.08	0.31	−1.87	0.14	−0.005	0.025
25	8.63	−1.43	0.16	−4.98	0.10	−0.053	0.025
25	9.78	−0.45	0.13	−3.46	0.09	−0.030	0.011
25	10.45	−0.01	0.03	−1.31	0.08	0.006	0.012
25	11.45	0.14	0.07	−0.05	0.09	0.001	0.025
40	8.38	−1.28	0.18	−4.72	0.06	−0.046	0.024
40	11.41	0.09	0.06	0.18	0.15	−0.015	0.033
60	8.3	−0.58	0.08	−4.21	0.04	−0.029	0.020
60	11.28	0.22	0.07	0.00	0.02	0.006	0.011

[a]1 SD refers to 1 standard deviation propagated from the isotopic analytical error in each individual experiment.

$\Delta\delta^{13}C_{BaCO_3-DIC}$, $\Delta\delta^{18}O_{BaCO_3-DIC}$, and $\Delta\Delta_{47\,BaCO_3-DIC}$ values varied significantly with increasing temperature at pH 8.30–8.63 (Figure 3). In these experiments, the solutions contained predominantly HCO_3^-. For the other experiments the temperature dependence is less clear. KFF magnitudes generally decreased with increasing pH, as clearly indicated by 25°C experiments (Figure 3). At pH 11.28–11.45, $\Delta\delta^{13}C_{BaCO_3-DIC}$ values were close to 0‰ within error at all temperatures (Figure 3a), suggesting that the KIE during $BaCO_3$ precipitation from CO_3^{2-}-dominated solutions led to negligible fractionation in ^{13}C. For oxygen and clumped isotopes, the KFFs associated with CO_3^{2-}-dominated solutions were also close to 0‰ within error (Figures 3b and 3c), although this was not the case for $\Delta\delta^{18}O_{BaCO_3-DIC}$ at 15°C, where the KFF was −1.87‰ ± 0.14‰ (Figure 3b).

4. Discussion

4.1. Comparison With Previously Published KFFs

4.1.1. Carbon Isotopes

Watkins and Hunt (2015) suggested that ^{13}C KFFs of HCO_3^- and CO_3^{2-} ($\Delta\delta^{13}C_{BaCO_3-HCO_3^-}$ and $\Delta\delta^{13}C_{BaCO_3-CO_3^{2-}}$) are close to zero, based on an ion-by-ion calcite growth model for carbon isotopes. Although these KFFs were not measured experimentally, the Watkins and Hunt (2015)'s model (WH15 model hereafter) indicated that the $\delta^{13}C$ value of calcite precipitated at pH 8.3 decreases with increasing calcite growth rate relative to an equilibrium isotopic composition inferred from Bottinga (1968) and Coplen (2007), and is close to zero relative to the $\delta^{13}C$ value of HCO_3^- at the rapid growth limit. This growth-related ^{13}C fractionation pattern is broadly consistent with $\delta^{13}C$ values of some inorganic calcites precipitated at 25°C (Levitt et al., 2018; Romanek et al., 1992). However, our results indicate that ^{13}C KFF of HCO_3^- is −1.43‰ at 25°C and have a weak temperature dependence (<~0.02‰°C^{-1}, Figures 4a and 4b), suggesting that calcite precipitated from a HCO_3^--dominated solution at rapid rates may have a $\delta^{13}C$ value lower than previously thought. Our experimentally determined KFFs are more comparable with those of Sade et al. (2020), with both studies indicating the same fractionation direction and differing slightly (less than ~0.3‰) in magnitude relative to 0‰ (zero KIE). Experiments of Sade et al. (2020) involved $BaCO_3$ FP in a finite DIC reservoir with solution chemistry varying significantly during precipitation; KFFs were determined using a dynamic model to account for this variability with several input parameters and related uncertainties taken into account. However, as stated in Sade et al. (2020)'s study, their modeled $\delta^{13}C$ values in $BaCO_3$ based on their best fit KFF showed significant deviations from their measured samples, which could be explained by atmospheric CO_2 contamination. Although our experiments were also potentially subjected to the CO_2 contamination, especially during the filtrating and drying when atmospheric CO_2 could have dissolved and precipitated as $BaCO_3$ with a different $\delta^{13}C$ value, the two QP experiments before and after each FP experiment are designed to monitor and correct for the potential contamination. This approach is different from Sade et al. (2020)'s method, possibly explaining the minor offsets in the fractionation magnitude between the two studies (Figure 4).

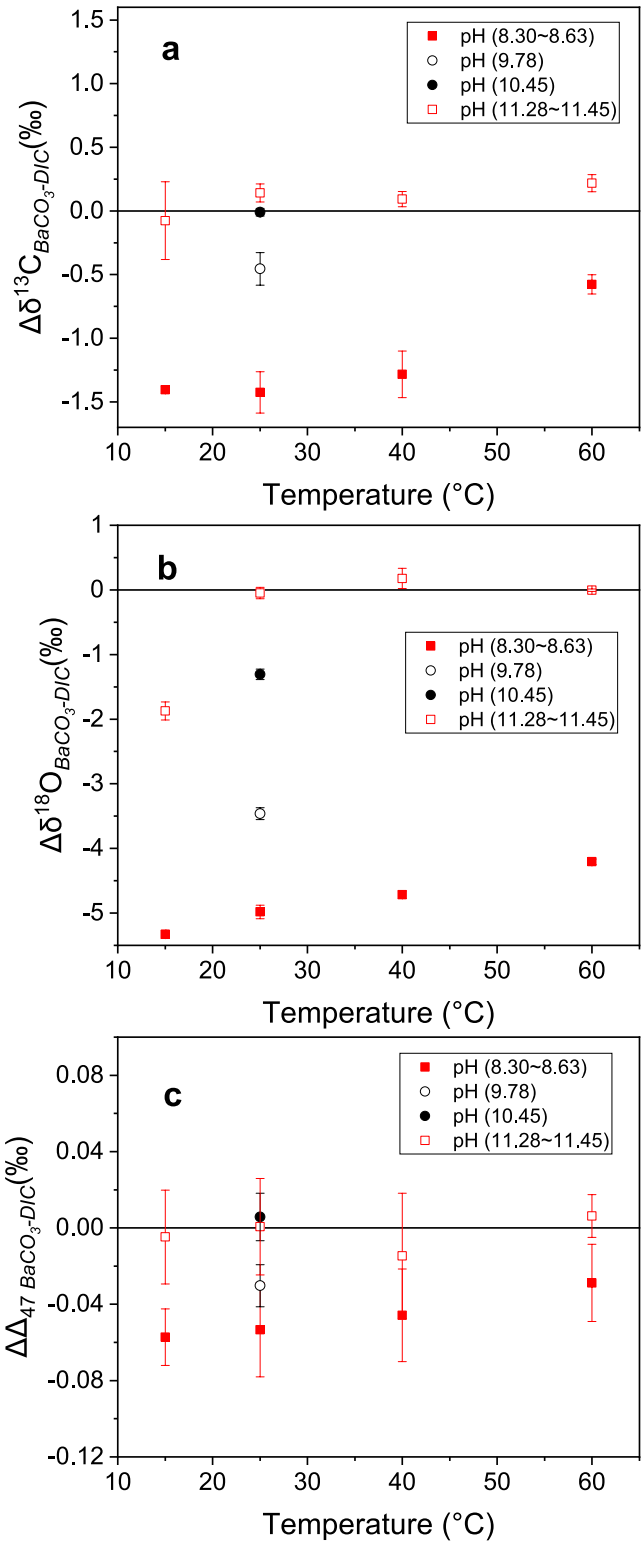

Figure 3. Temperature dependence of kinetic fractionation factors during $BaCO_3$ growth under different pH values for (a) carbon, (b) oxygen, and (c) clumped isotopes.

4.1.2. Oxygen Isotopes

Kim et al. (2006) determined the ^{18}O KIE during carbonate precipitation at 25°C, based on $BaCO_3$ FP. However, the ^{18}O KFFs between $BaCO_3$ and DIC species ($\Delta\delta^{18}O_{BaCO_3-HCO_3^-}$ and $\Delta\delta^{18}O_{BaCO_3-CO_3^{2-}}$) were subject to the Rayleigh distillation effect as their $BaCO_3$ samples were formed in a finite DIC reservoir. Devriendt et al. (2017) developed a model to account for Rayleigh distillation and derived the $\Delta\delta^{18}O_{BaCO_3-HCO_3^-}$ and $\Delta\delta^{18}O_{BaCO_3-CO_3^{2-}}$ values of $-5.0 \pm 0.2‰$ and the $-0.5 \pm 0.2‰$, respectively. These KFFs are broadly consistent with those reported by Sade et al. (2020) and determined at the same temperature in this study (Figures 4c and 4d). Regarding the dependence of KIEs on temperature, we found that $\Delta\delta^{18}O_{BaCO_3-HCO_3^-}$ values are temperature-dependent between 15 and 60°C, while $\Delta\delta^{18}O_{BaCO_3-CO_3^{2-}}$ values are not (at 25°C–60°C; at 15°C a more negative $\Delta\delta^{18}O_{BaCO_3-CO_3^{2-}}$ value was observed). These results are generally comparable with those of Sade et al. (2020). The presence and absence of the dependence of the KIEs on temperature are elusive. They may be related to the possible variation in $BaCO_3$ precipitation rates, which are correlated positively with temperature at the same pH and solubility product, although the precipitation here is rapid on the scale of a few seconds time. The higher temperature may promote a more significant local precipitation of $BaCO_3$ at solution surface after injecting the $BaCl_2$ into the solution, allowing the precipitation of DIC species at the surface to be more quantitative than fractional. This effect can reduce the magnitude of the KIEs, leading to the dependence of the KIEs on temperature. This effect may also be minimized by a higher Ba^{2+} ion diffusion rate at the higher temperature if the diffusion surpassed the precipitation rate, then possibly explaining the missing of the dependence. Future studies are needed to better constrain the $BaCO_3$ precipitation rate and verify the effect using $BaCl_2$ solutions with different concentrations or varying the solution stirring rate.

Based on the ion-by-ion growth model, Watkins et al. (2014) fitted KFFs associated with calcite growth by the data of experimental calcites precipitated at 25°C with various pH values and growth rates, resulting in $\Delta\delta^{18}O_{BaCO_3-HCO_3^-}$ and $\Delta\delta^{18}O_{BaCO_3-CO_3^{2-}}$ values of $-3.6‰$ and $-2.0‰$, respectively. These estimates on ^{18}O KFFs differ significantly from our experimental results, especially for the ^{18}O KFF of CO_3^{2-}. The difference (Figure 4d) is not surprising as the ^{18}O KFF of CO_3^{2-} is more difficult to constrain than that of HCO_3^- because the isotopic equilibration of DIC solution is extremely slow at high pH (Uchikawa & Zeebe, 2013; Watkins et al., 2014). The potential mineralogical effect on KFFs between calcite and witherite may not be important as the KFFs in this study were determined by the difference of isotopic values obtained from different $BaCO_3$ precipitation experiments. Additionally, the KIE associated with $BaCO_3$ precipitation was revealed by precipitating fractional DIC species in solution with low $[Ba^{2+}]/[DIC]$ ratio. This means that the large amount of DIC species may compete to attach with cations or on the crystal surface where the mass-dependent transports of the DIC species are involved (DePaolo, 2011; Mills et al., 2021). The kinetic isotopic fractionation of DIC species may take place mainly during this process, and should be not affected by the mineralogy of final precipitates. Considering the similarity between results of this study and those of Sade et al. (2020), we suggest that these experimentally determined ^{18}O KFFs may be more reliable than those constrained by Watkins et al. (2014). These KFFs should be incorporated in the WH15 model to see how the modeled rate-dependence of $\delta^{18}O$

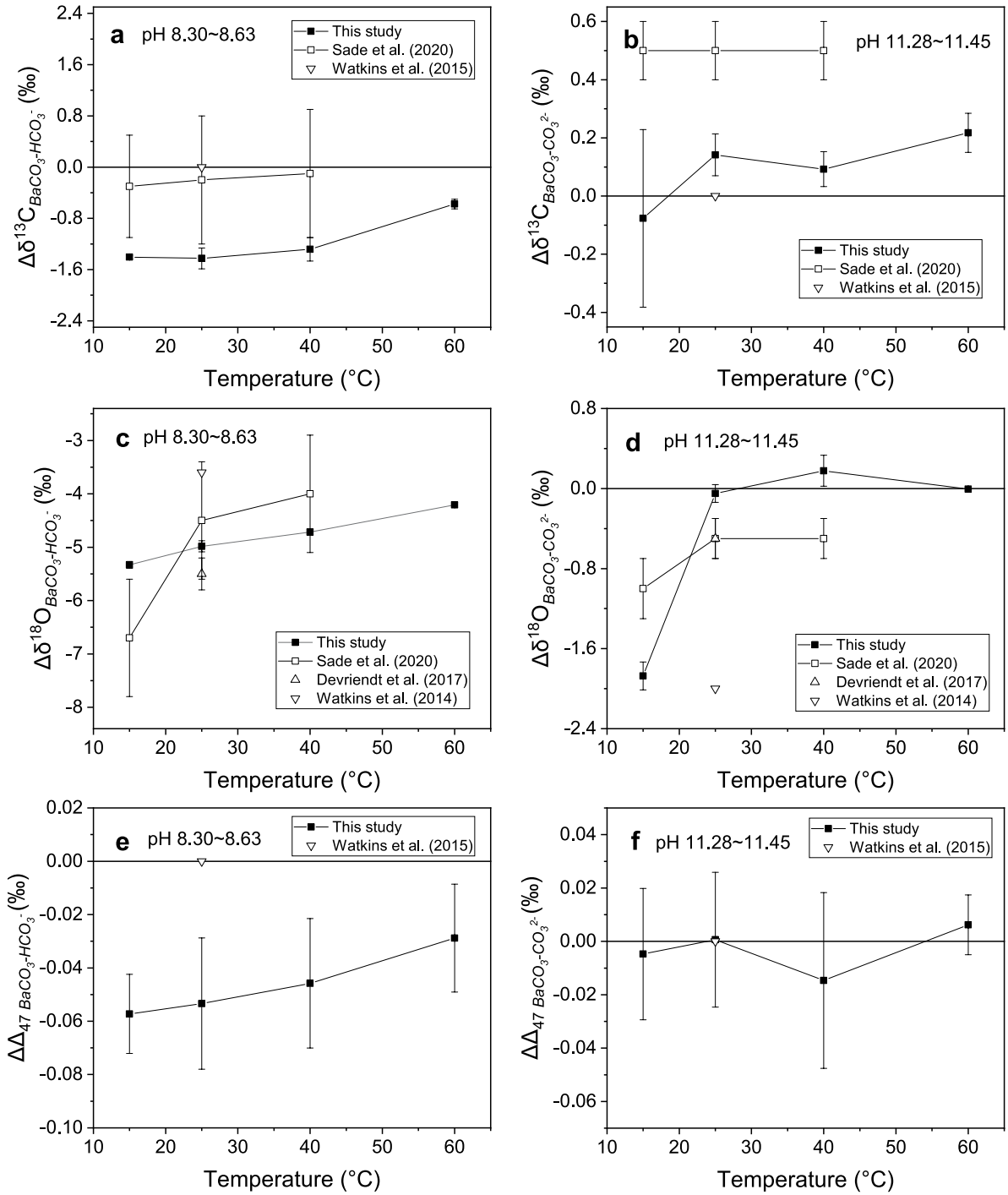

Figure 4. Comparison of kinetic fractionation factors with those reported previously (Devriendt et al., 2017; Sade et al., 2020; Watkins & Hunt, 2015; Watkins et al., 2014) for (a and b) carbon, (c and d) oxygen, and (e and f) clumped isotopes.

compares with existing or ongoing experimental studies where DIC solutions are isotopically equilibrated before carbonate precipitations.

4.1.3. Clumped Isotopes

The WH15 model, modified and extended to clumped isotopes, suggests little or no KIE for HCO_3^- ($\Delta\Delta_{47\,BaCO_3-HCO_3^-}$) and CO_3^{2-} ($\Delta\Delta_{47\,BaCO_3-CO_3^{2-}}$) during calcite growth (Watkins & Hunt, 2015). This means that the

Δ_{47} value for rapid-growth calcite depends mainly on the weighted sum of Δ_{47} values of the DIC species involved. It should be noted that an isotopic mixing of DIC species with different bulk isotopic compositions can cause significant offset in Δ_{47} values after the DIC species are quantitatively precipitated (Thiagarajan et al., 2011). Although the WH15 model also suggests that there can be a significant difference (>0.01‰) on Δ_{47} values between equilibrium calcite and the disequilibrium calcite in case of rapid crystallization with fractionation directions depending on how to specify KFFs as the model input parameters, which has not yet been validated by reliable experimental Δ_{47} data.

Tang et al. (2014) conducted calcite precipitation experiments with different precipitation rates at constant pH and ionic strength, and found no clear effects of precipitation rates on Δ_{47} values, suggesting that KIE associated with crystal growth may be unimportant for most natural carbonates. However, according to the WH15 model, the absence of KIE may be attributed to the narrow range of calcite growth rates considered, with calcite formation not having approached its kinetic limit (and with KIE associated with rapid-growth therefore not appearing). Nevertheless, the WH15 model and Tang et al. (2014)'s results would be consistent with ours at 25°C for calcite grown in a CO_3^{2-}-dominated solution, for which we found that the $\Delta\Delta_{47\,BaCO_3-CO_3^{2-}}$ value is close to zero (Figure 4f). However, in a HCO_3^--dominated solution, our $\Delta\Delta_{47\,BaCO_3-HCO_3^-}$ value indicates that the KIE due to calcite growth results in lower Δ_{47} values, especially at lower temperatures (Figure 4e). The negative Δ_{47} fractionation associated with KIE is consistent with observation of natural carbonates in previous studies (Herlambang & John, 2021; Loyd et al., 2016; Thiagarajan et al., 2020). For example, modern seep carbonates exhibit anomalously low Δ_{47} values, possibly due to rapid carbonate precipitation (Loyd et al., 2016; Thiagarajan et al., 2020). de Winter et al. (2021) found that the chalky microstructures of the oyster shells with high growth rates show lower Δ_{47} values compared with the foliated microstructure with low growth rates. Herlambang and John (2021) applied trace-element partitioning in constraining the precipitation rate of natural calcites and found that samples with higher precipitation rates have lower Δ_{47} values. Provided that the variation of Δ_{47} values in their macro-columnar calcites was controlled primarily by KIE during calcite growth, the highest magnitude of Δ_{47} fractionation would be ~0.05‰, broadly comparable with the range of KFFs determined in our study (Figure 4e). These results suggest that to predict a rate dependence of Δ_{47} values for carbonates by the WH15 model, the input parameters require that the KFFs between HCO_3^- and carbonate mineral are not equal to zero.

4.2. HCO_3^- and CO_3^{2-} Precipitation Pathways

KFFs determined in this study may be useful in distinguishing between contributions of HCO_3^- and CO_3^{2-} to carbonate growth. If there is a preference for a particular DIC species to be incorporated during carbonate growth, the final isotopic disequilibrium in carbonates may be superimposed with the disequilibrated compositions of the preferred DIC species. The KFF values themselves are also possibly subjected to such preferred incorporation. A simple hypothesis is that the rapid $BaCl_2$ titration of a small fraction of the DIC in the FP experiments strongly selects for CO_3^{2-} in the HCO_3^--dominated solution. If so, the $\delta^{13}C$, $\delta^{18}O$, and Δ_{47} values of $BaCO_3$ formed from FP would be lower than those formed from QP with DIC solution being equilibrated, as the equilibrium $\delta^{13}C$, $\delta^{18}O$, and Δ_{47} values of CO_3^{2-} are known to be significantly lower than those of HCO_3^- (Beck et al., 2005; Tripati et al., 2015; Uchikawa & Zeebe, 2013; Zhang et al., 1995). These fractionation signatures agree with the negative $\Delta\delta^{18}O_{BaCO_3-HCO_3^-}$, $\Delta\delta^{13}C_{BaCO_3-HCO_3^-}$, and $\Delta\Delta_{47\,BaCO_3-HCO_3^-}$ values determined in this study (Figures 4a, 4c, and 4e). However, Zhang et al. (1995) experimentally determined the equilibrium fractionation between different DIC species and suggested that the equilibrated $\delta^{13}C$ value of CO_3^{2-} is lower than that of HCO_3^- by ~2.6‰ at 15°C and ~2.0‰ at 25°C. These fractionation magnitudes and temperature dependency are not consistent with the $\Delta\delta^{13}C_{BaCO_3-HCO_3^-}$ values (Figure 4a; Table 2) determined in this study, even if the Ba^{2+} dissolved in DIC solutions from the FP experiments only selects for CO_3^{2-}. According to the hypothesis of preferred incorporation of CO_3^{2-}, the isotopic compositions of the partial and quantitative precipitation experiments should be close in the CO_3^{2-}-dominated solutions, which is inconsistent with the negative $\Delta\delta^{18}O_{BaCO_3-CO_3^{2-}}$ value determined in this study and those determined by Sade et al. (2020) (Figure 4d). Consequently, the KFFs determined in either HCO_3^- or CO_3^{2-}-dominated solutions are unlikely involved with the preferred incorporation for a particular DIC species. They mainly reflect KIEs associated with the process of irreversible transfer of DIC species from the solution to the solid.

The preference for a particular DIC species during carbonate growth may be observable in DIC solutions with various pH values or $[CO_3^{2-}]$/[DIC] ratios. For example, in aragonite precipitation experiments in isotopically

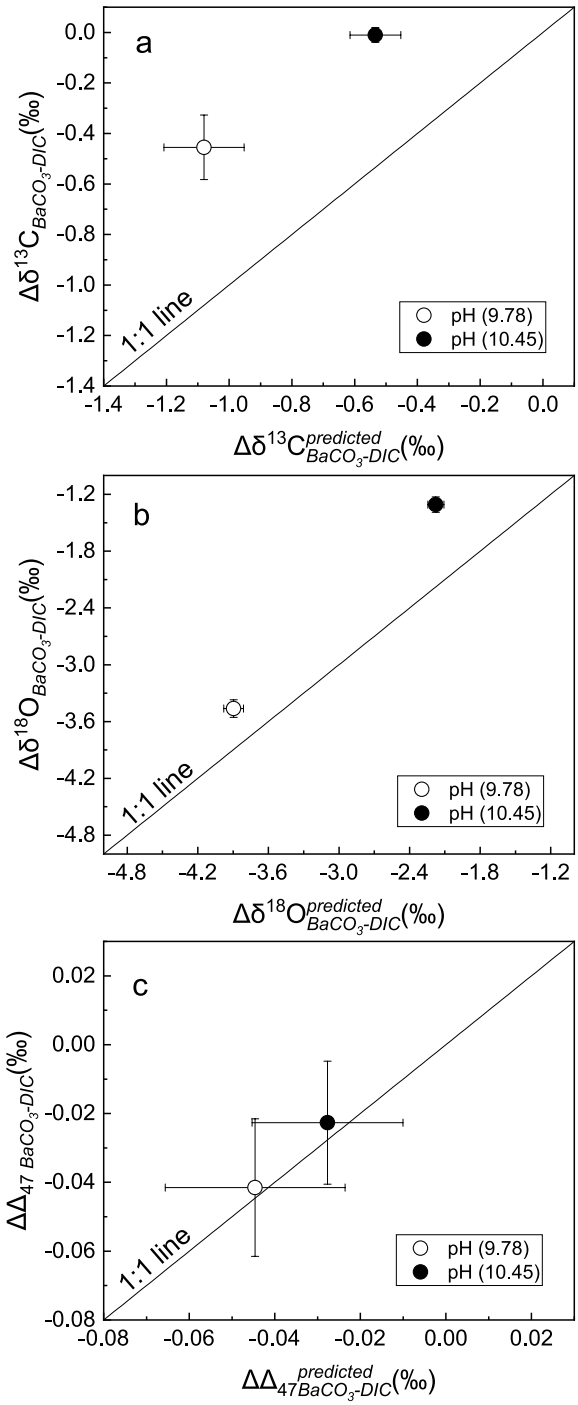

Figure 5. Comparison of measured and predicted kinetic fractionation factors (KFFs) associated with rapid $BaCO_3$ growth at 25°C, for (a) carbon, (b) oxygen, and (c) clumped isotopes. Predicted KFFs were calculated by the KFFs measured at CO_3^{2-}- and HCO_3^--dominated dissolved inorganic carbon (DIC) solutions, weighted by proportions of the two DIC species in solution (see text for detail).

equilibrated DIC solutions at 25°C with a pH range of 8.25–10.75 corresponding to $[CO_3^{2-}]$/[DIC] ratios from 3% to 91%, Kim et al. (2006) found that $\delta^{18}O$ values of rapid-growth aragonites were between the equilibrated values of aragonite and CO_3^{2-} ions, suggesting that the CO_3^{2-} ion indeed preferentially contributed to aragonite growth relative to the HCO_3^- ion. To test such a preference, we compared the KFFs determined in the FP experiments at 25°C and pH 9.78–10.45 with those predicted assuming no preference for HCO_3^- and CO_3^{2-} in carbonate growth. Predicted KFFs for carbon, oxygen, and clumped isotopes were calculated as follows:

$$\Delta\delta^{13}C^{predicted}_{BaCO_3-DIC} = f_{B1}\Delta\delta^{13}C_{BaCO_3-CO_3^{2-}} + f_{B2}\Delta\delta^{13}C_{BaCO_3-HCO_3^-} \quad (6)$$

$$\Delta\delta^{18}O^{predicted}_{BaCO_3-DIC} = f_{B1}\Delta\delta^{18}O_{BaCO_3-CO_3^{2-}} + f_{B2}\Delta\delta^{18}O_{BaCO_3-HCO_3^-} \quad (7)$$

$$\Delta\Delta^{predicted}_{47\,BaCO_3-DIC} = f_{B1}\Delta\Delta_{47\,BaCO_3-CO_3^{2-}} + f_{B2}\Delta\Delta_{47\,BaCO_3-HCO_3^-} \quad (8)$$

where f_{B1} and f_{B2} are $[CO_3^{2-}]$/[DIC] and $[HCO_3^-]$/[DIC] ratios, respectively. Note that significant variations in $\delta^{13}C$ and $\delta^{18}O$ values between the two population of DIC species could cause offsets in Δ_{47} values due to the non-linear mixing effect (Defliese & Lohmann, 2015; Eiler & Schauble, 2004). To evaluate these possible offsets, we used a mixing model from Wang et al. (2015) to calculate the non-linear mixed Δ_{47} values. The calculated offsets of the non-linear mixed Δ_{47} values from the $\Delta\Delta^{predicted}_{47\,BaCO_3-DIC}$ value are only ~0.002‰, which are within the analytical error and negligible. The KFFs determined for all isotopic systems addressed in this study are significantly higher than those predicted (Figure 5), except for Δ_{47} whose KFFs are indistinguishable from those predicted due to the large propagated error. Nevertheless, these comparisons suggest that CO_3^{2-} ions with less-negative KFFs preferentially contribute to carbonate growth relative to HCO_3^- ions, consistent with the results of Kim et al. (2006). This also means that the KFFs determined at pH values of 9.78 and 10.45 were superimposed with the isotopic compositions of the preferred CO_3^{2-} ions.

The mechanism of the preference for the CO_3^{2-} precipitation pathway is less clear. It may be associated with an extra thermodynamic driving force for this pathway. Andersson et al. (2016) calculated the adsorption energy of CO_3^{2-} or HCO_3^- ions from aqueous solution onto calcite surface using density functional theory and found that the adsorption free energy of CO_3^{2-} is significantly lower than that of HCO_3^-. This means that the CO_3^{2-} is preferentially adsorbed on calcite over HCO_3^-, possibly leading to higher surface concentration of CO_3^{2-} than adsorbed HCO_3^-. This theoretical prediction agrees with the surface complexation model, which shows that the surface concentration of CO_3^{2-} on calcite is dozens of times higher than that of HCO_3^- at a HCO_3^--dominated solution (Pokrovsky et al., 2000). Note that this remarkably high surface concentration of CO_3^{2-} does not necessarily suggest that carbonate precipitates from CO_3^{2-} exclusively in the bulk solution because the absorbed CO_3^{2-} can be partly derived from the HCO_3^- in the solution by rapid deprotonation to CO_3^{2-}. Otherwise, the isotopic composition of carbonate would reflect solely that of CO_3^{2-} consumed during precipitation.

4.3. Clumped Isotope Disequilibrium in Natural Carbonates

The KIEs observed here in $BaCO_3$ precipitations may aid the understanding of Δ_{47} disequilibrium that commonly occurs in natural carbonates. Several

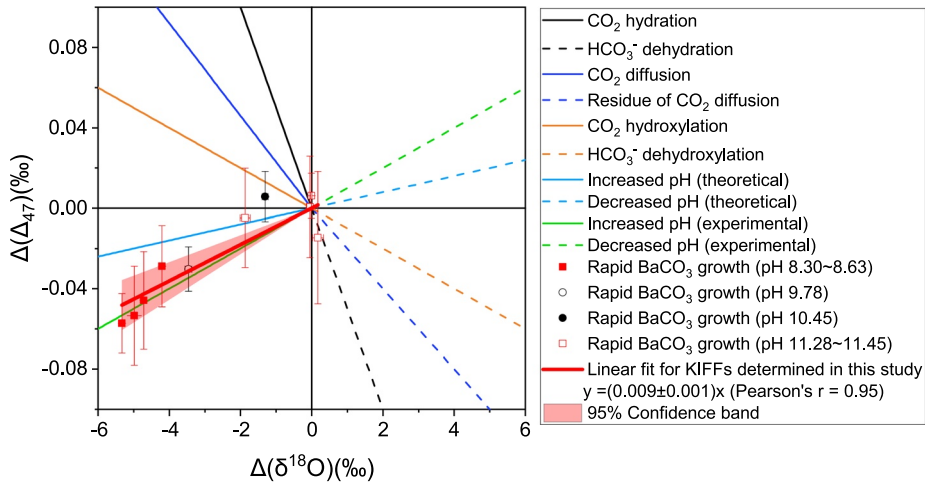

Figure 6. Disequilibrium of oxygen and clumped isotopes controlled by various factors, each of which displays a distinct fractionation relationship between $\delta^{18}O$ and Δ_{47}. CO_2 hydration and hydroxylation result in an increase in Δ_{47} and a decrease in $\delta^{18}O$ values (Guo, 2020; Saenger et al., 2012). CO_2 hydration and HCO_3^- dehydration have the same $\Delta(\Delta_{47})/\Delta(\delta^{18}O)$ slopes, but with the inverse fractionation directions, so do the CO_2 hydroxylation and HCO_3^- dehydroxylation (Guo, 2020; Saenger et al., 2012). CO_2 diffusion in the liquid phase results in an increase in Δ_{47} and a decrease in $\delta^{18}O$ values, with the CO_2 residue having low Δ_{47} and high $\delta^{18}O$ values (Thiagarajan et al., 2011). Theoretical (Hill et al., 2014) and experimental (Tripati et al., 2015) studies indicate higher Δ_{47} and $\delta^{18}O$ values at lower pH and vice versa. Kinetic fractionation factors associated with the rapid $BaCO_3$ growth in this study lead to lower Δ_{47} and $\delta^{18}O$ values, with more disequilibrium at lower pH.

factors play important roles in defining Δ_{47} disequilibrium signatures in carbonates, including DIC speciation (the "pH effect"; Hill et al., 2014; Tripati et al., 2015), KIEs associated with CO_2 hydration/hydroxylation (Guo, 2020; Saenger et al., 2012) and HCO_3^- dehydration/dehydroxylation (Affek & Zaarur, 2014; Daëron et al., 2011; Falk et al., 2016; Guo & Zhou, 2019), and CO_2 diffusion (Eiler & Schauble, 2004; Thiagarajan et al., 2011). These factors induce specific correlations between Δ_{47} and $\delta^{18}O$ values, with distinct $\Delta(\Delta_{47})/\Delta(\delta^{18}O)$ slopes, which may indicate the factors involved and explain the predominant mechanism of carbonate isotopic disequilibrium (Figure 6). The $\Delta(\Delta_{47})$ and $\Delta(\delta^{18}O)$ values indicate degrees in carbonate isotopic disequilibrium relative to specific equilibria, and are usually defined by deviations in isotopic compositions from expected equilibrium values.

To obtain the $\Delta(\Delta_{47})/\Delta(\delta^{18}O)$ slope specific to KIE associated with rapid $BaCO_3$ growth, we assigned the $\Delta(\Delta_{47})$ and $\Delta(\delta^{18}O)$ values to $\Delta\Delta_{47\,BaCO_3-DIC}$ and $\Delta\delta^{18}O_{BaCO_3-DIC}$, respectively, as determined under different experimental conditions. Linear fitting with zero intercept by the weighted least-square method (OriginPro software, 2018) was undertaken to calculate the $\Delta(\Delta_{47})/\Delta(\delta^{18}O)$ slope. In the $\Delta(\Delta_{47})$–$\Delta(\delta^{18}O)$ diagram (Figure 6), $\Delta(\Delta_{47})$ values increase with increasing $\Delta(\delta^{18}O)$ values, suggesting that a high growth rate leads to decreases in both Δ_{47} and $\delta^{18}O$ values. The slope (0.011 ± 0.003) is similar to that for pH-driven isotopic disequilibrium determined experimentally (Tripati et al., 2015). The pH effect may not account for KIEs associated with rapid $BaCO_3$ growth, as more negative Δ_{47} and $\delta^{18}O$ values (due to the pH effect) would be expected at higher $[CO_3^{2-}]/[HCO_3^-]$ ratios (at higher pH). However, our data indicate that lower Δ_{47} and $\delta^{18}O$ values are more likely at lower $[CO_3^{2-}]/[HCO_3^-]$ ratios (at lower pH; Figure 6). It is true that a strong preferential incorporation of the equilibrated CO_3^{2-} relative to HCO_3^- will also lead to a fractionation pattern similar to the pH effect. The KFFs determined at pH values of 9.78 and 10.45 could be the example. However, as the KFFs determined in HCO_3^- or CO_3^{2-}-dominated solutions are unlikely involved with the preference effect, we surmise that the $\Delta(\Delta_{47})/\Delta(\delta^{18}O)$ slope cannot be attributed to pH effect, but mainly reflects the growth-related KIE. It follows that the identification of KIEs associated with higher precipitation rates in natural carbonates, based on the slopes determined here, requires knowledge of fluid pH conditions in which carbonate growth occurs. It also requires that the carbonate growth rate should approach the kinetic limit. If the precipitation fluid has a high $[Ca^{2+}]/[DIC]$ concentration ratio or DIC species are not fractionally precipitated, the KIEs may not be apparent. If the isotopic disequilibrium of carbonate samples is deemed to relate merely to the rapid growth rate at different levels, their $\Delta(\Delta_{47})$ and $\Delta(\delta^{18}O)$ values should lie between the highest disequilibrium and equilibrium values, on the slope of the $\Delta(\Delta_{47})/\Delta(\delta^{18}O)$ line as determined

here. In case that the equilibrium values are unknown, the Δ_{47} and $\delta^{18}O$ values of the samples may be offset from but still parallel to the $\Delta(\Delta_{47})/\Delta(\delta^{18}O)$ slope. These predictions need to be tested in future studies by analyzing rapid-growth natural carbonates whose expected equilibrium Δ_{47} and $\delta^{18}O$ values are well constrained. As the degree of fractionation caused by KIEs is more sensitive to pH than temperature, the $\Delta(\Delta_{47})/\Delta(\delta^{18}O)$ slope may potentially be applied to marine carbonates precipitated at normal seawater pH values over temperature range of 15–60°C. If the $\Delta_{47}/\delta^{18}O$ ratios of these carbonates exhibit the similar slope as determined here, it will be reasonable to reconstruct their formation temperature using the highest Δ_{47} value of the sample as it may be less affected by the growth-related KIE.

5. Conclusions

Based on a series of $BaCO_3$ precipitation experiments, this study presents evidence of KIEs associated with carbonate growth for carbon, oxygen, and clumped isotopes. A set of KFFs derived for CO_3^{2-} and HCO_3^- precipitation indicate that rapid carbonate growth can lead to lower $\delta^{13}C$, $\delta^{18}O$, and Δ_{47} values in HCO_3^--dominated solutions, with more fractionation at lower temperatures. KFFs for $\delta^{13}C$ and $\delta^{18}O$ are broadly comparable with previous experimental estimates in terms of the direction and temperature dependence of the fractionation, despite differences in fractionation magnitude. These experimental determined KFFs can help to constrain the growth rate dependence of isotopic compositions in carbonate by the WH15 model. Our data verified a preference for the CO_3^{2-} pathway during carbonate precipitation, with important implications for earlier isotopic disequilibrium models (Watkins & Hunt, 2015; Zeebe, 1999) that assume no preference between DIC species in carbonate precipitation. Our findings provide a fractionation pattern for $\delta^{18}O$ and Δ_{47} that may be useful in identifying KIEs associated with high carbonate growth rates and in elucidating isotopic disequilibrium of natural carbonate formed at temperature and pH ranges of 15–60°C and 8.3–11.5, respectively.

Conflict of Interest

The authors declare no conflicts of interest relevant to this study.

Data Availability Statement

The supporting materials including raw data are available on Zenodo (https://dx.doi.org/10.5281/zenodo.5115321).

Acknowledgments
This study was supported by the National Natural Science Foundation of China (41722301, 42003001, 42173016, 41973003, 42021002), and the Key Special Project for Introduced Talents Team of Southern Marine Science and Engineering Guangdong Laboratory (Guangzhou) (GML2019ZD0206). The authors like to thank two anonymous reviewers for their constructive suggestions and comments. The English of the manuscript was improved by Stallard Scientific Editing. This is contribution No. IS – 3147 from GIGCAS.

References

Affek, H. P., & Zaarur, S. (2014). Kinetic isotope effect in CO_2 degassing: Insight from clumped and oxygen isotopes in laboratory precipitation experiments. *Geochimica et Cosmochimica Acta*, *143*, 319–330. https://doi.org/10.1016/j.gca.2014.08.005

Andersson, M. P., Rodriguez-Blanco, J. D., & Stipp, S. L. S. (2016). Is bicarbonate stable in and on the calcite surface? *Geochimica et Cosmochimica Acta*, *176*, 198–205. https://doi.org/10.1016/j.gca.2015.12.016

Beck, W. C., Grossman, E. L., & Morse, J. W. (2005). Experimental studies of oxygen isotope fractionation in the carbonic acid system at 15°, 25°, and 40°C. *Geochimica et Cosmochimica Acta*, *69*(14), 3493–3503. https://doi.org/10.1016/j.gca.2005.02.003

Bernasconi, S. M., Daeron, M., Bergmann, K. D., Bonifacie, M., Meckler, A. N., Affek, H. P., et al. (2021). InterCarb: A community effort to improve interlaboratory standardization of the carbonate clumped isotope thermometer using carbonate standards. *Geochemistry, Geophysics, Geosystems*, *22*(5), e2020GC009588. https://doi.org/10.1029/2020gc009588

Bottinga, Y. (1968). Calculation of fractionation factors for carbon and oxygen isotopic exchange in the system calcite-carbon dioxide-water. *The Journal of Physical Chemistry*, *72*(3), 800–808. https://doi.org/10.1021/j100849a008

Brand, W. A., Assonov, S. S., & Coplen, T. B. (2010). Correction for the ^{17}O interference in $\delta(^{13}C)$ measurements when analyzing CO_2 with stable isotope mass spectrometry (IUPAC Technical Report). *Pure and Applied Chemistry*, *82*(8), 1719–1733. https://doi.org/10.1351/pac-rep-09-01-05

Coplen, T. B. (2007). Calibration of the calcite–water oxygen-isotope geothermometer at Devils Hole, Nevada, a natural laboratory. *Geochimica et Cosmochimica Acta*, *71*(16), 3948–3957. https://doi.org/10.1016/j.gca.2007.05.028

Daëron, M., Blamart, D., Peral, M., & Affek, H. P. (2016). Absolute isotopic abundance ratios and the accuracy of Δ_{47} measurements. *Chemical Geology*, *442*, 83–96. https://doi.org/10.1016/j.chemgeo.2016.08.014

Daëron, M., Drysdale, R. N., Peral, M., Huyghe, D., Blamart, D., Coplen, T. B., et al. (2019). Most Earth-surface calcites precipitate out of isotopic equilibrium. *Nature Communications*, *10*(1), 429. https://doi.org/10.1038/s41467-019-08336-5

Daëron, M., Guo, W., Eiler, J., Genty, D., Blamart, D., Boch, R., et al. (2011). $^{13}C^{18}O$ clumping in speleothems: Observations from natural caves and precipitation experiments. *Geochimica et Cosmochimica Acta*, *75*(12), 3303–3317. https://doi.org/10.1016/j.gca.2010.10.032

Defliese, W. F., & Lohmann, K. C. (2015). Non-linear mixing effects on mass-47 CO_2 clumped isotope thermometry: Patterns and implications. *Rapid Communications in Mass Spectrometry*, *29*(9), 901–909. https://doi.org/10.1002/rcm.7175

Dennis, K. J., Affek, H. P., Passey, B. H., Schrag, D. P., & Eiler, J. M. (2011). Defining an absolute reference frame for 'clumped' isotope studies of CO_2. *Geochimica et Cosmochimica Acta*, *75*(22), 7117–7131. https://doi.org/10.1016/j.gca.2011.09.025

Dennis, K. J., Cochran, J. K., Landman, N. H., & Schrag, D. P. (2013). The climate of the Late Cretaceous: New insights from the application of the carbonate clumped isotope thermometer to Western Interior Seaway macrofossil. *Earth and Planetary Science Letters*, *362*, 51–65. https://doi.org/10.1016/j.epsl.2012.11.036

DePaolo, D. J. (2011). Surface kinetic model for isotopic and trace element fractionation during precipitation of calcite from aqueous solutions. *Geochimica et Cosmochimica Acta*, *75*(4), 1039–1056. https://doi.org/10.1016/j.gca.2010.11.020

Devriendt, L. S., Watkins, J. M., & McGregor, H. V. (2017). Oxygen isotope fractionation in the $CaCO_3$-DIC-H_2O system. *Geochimica et Cosmochimica Acta*, *214*, 115–142. https://doi.org/10.1016/j.gca.2017.06.022

de Winter, N. J., Dammer, L. K., Falkenroth, M., Reichart, G. J., Moretti, S., Martinez-Garcia, A., et al. (2021). Multi-isotopic and trace element evidence against different formation pathways for oyster microstructures. *Geochimica et Cosmochimica Acta*, *308*, 326–352. https://doi.org/10.1016/j.gca.2021.06.012

Eiler, J. M. (2007). "Clumped-isotope" geochemistry—The study of naturally-occurring, multiply-substituted isotopologues. *Earth and Planetary Science Letters*, *262*(3–4), 309–327. https://doi.org/10.1016/j.epsl.2007.08.020

Eiler, J. M. (2011). Paleoclimate reconstruction using carbonate clumped isotope thermometry. *Quaternary Science Reviews*, *30*(25–26), 3575–3588. https://doi.org/10.1016/j.quascirev.2011.09.001

Eiler, J. M., & Schauble, E. (2004). $^{18}O^{13}C^{16}O$ in Earth's atmosphere. *Geochimica et Cosmochimica Acta*, *68*(23), 4767–4777. https://doi.org/10.1016/j.gca.2004.05.035

Falk, E. S., Guo, W., Paukert, A. N., Matter, J. M., Mervine, E. M., & Kelemen, P. B. (2016). Controls on the stable isotope compositions of travertine from hyperalkaline springs in Oman: Insights from clumped isotope measurements. *Geochimica et Cosmochimica Acta*, *192*, 1–28. https://doi.org/10.1016/j.gca.2016.06.026

Fernandez, A., Korte, C., Ullmann, C. V., Looser, N., Wohlwend, S., & Bernasconi, S. M. (2021). Reconstructing the magnitude of Early Toarcian (Jurassic) warming using the reordered clumped isotope compositions of belemnites. *Geochimica et Cosmochimica Acta*, *293*, 308–327. https://doi.org/10.1016/j.gca.2020.10.005

Finnegan, S., Bergmann, K., Eiler, J. M., Jones, D. S., Fike, D. A., Eisenman, I., et al. (2011). The magnitude and duration of Late Ordovician-Early Silurian glaciation. *Science*, *331*(6019), 903–906. https://doi.org/10.1126/science.1200803

Ghosh, P., Adkins, J., Affek, H., Balta, B., Guo, W., Schauble, E. A., et al. (2006). ^{13}C–^{18}O bonds in carbonate minerals: A new kind of paleothermometer. *Geochimica et Cosmochimica Acta*, *70*(6), 1439–1456. https://doi.org/10.1016/j.gca.2005.11.014

Guo, W. (2020). Kinetic clumped isotope fractionation in the DIC-H_2O-CO_2 system: Patterns, controls, and implications. *Geochimica et Cosmochimica Acta*, *268*, 230–257. https://doi.org/10.1016/j.gca.2019.07.055

Guo, W., & Zhou, C. (2019). Patterns and controls of disequilibrium isotope effects in speleothems: Insights from an isotope-enabled diffusion-reaction model and implications for quantitative thermometry. *Geochimica et Cosmochimica Acta*, *267*, 196–226. https://doi.org/10.1016/j.gca.2019.07.028

Guo, Y. R. (2021). Supplementary Dataset for "Experimental constraints on clumped isotope fractionation during BaCO3 precipitation" [Data set]. Zenodo. https://doi.org/10.5281/zenodo.5115321

Guo, Y. R., Deng, W. F., Liu, X., Kong, K., Yan, W., & Wei, G. J. (2021). Clumped isotope geochemistry of island carbonates in the South China Sea: Implications for early diagenesis and dolomitization. *Marine Geology*, *437*, 106513. https://doi.org/10.1016/j.margeo.2021.106513

Guo, Y. R., Deng, W. F., & Wei, G. J. (2019). Kinetic effects during the experimental transition of aragonite to calcite in aqueous solution: Insights from clumped and oxygen isotope signatures. *Geochimica et Cosmochimica Acta*, *248*, 210–230. https://doi.org/10.1016/j.gca.2019.01.012

Herlambang, A., & John, C. M. (2021). Combining clumped isotope and trace element analysis to constrain potential kinetic effects in calcite. *Geochimica et Cosmochimica Acta*, *296*, 117–130. https://doi.org/10.1016/j.gca.2020.12.024

Hill, P. S., Tripati, A. K., & Schauble, E. A. (2014). Theoretical constraints on the effects of pH, salinity, and temperature on clumped isotope signatures of dissolved inorganic carbon species and precipitating carbonate minerals. *Geochimica et Cosmochimica Acta*, *125*, 610–652. https://doi.org/10.1016/j.gca.2013.06.018

Huntington, K. W., Eiler, J. M., Affek, H. P., Guo, W., Bonifacie, M., Yeung, L. Y., et al. (2009). Methods and limitations of 'clumped' CO_2 isotope (Δ_{47}) analysis by gas-source isotope ratio mass spectrometry. *Journal of Mass Spectrometry*, *44*(9), 1318–1329. https://doi.org/10.1002/jms.1614

John, C. M., & Bowen, D. (2016). Community software for challenging isotope analysis: First applications of 'Easotope' to clumped isotopes. *Rapid Communications in Mass Spectrometry*, *30*(21), 2285–2300. https://doi.org/10.1002/rcm.7720

Kim, S. T., Hillaire-Marcel, C., & Mucci, A. (2006). Mechanisms of equilibrium and kinetic oxygen isotope effects in synthetic aragonite at 25°C. *Geochimica et Cosmochimica Acta*, *70*(23), 5790–5801. https://doi.org/10.1016/j.gca.2006.08.003

Kim, S. T., Mucci, A., & Taylor, B. E. (2007). Phosphoric acid fractionation factors for calcite and aragonite between 25 and 75°C: Revisited. *Chemical Geology*, *246*(3–4), 135–146. https://doi.org/10.1016/j.chemgeo.2007.08.005

Kim, S. T., & O'Neil, J. R. (1997). Equilibrium and nonequilibrium oxygen isotope effects in synthetic carbonates. *Geochimica et Cosmochimica Acta*, *61*(16), 3461–3475. https://doi.org/10.1016/s0016-7037(97)00169-5

Leutert, T. J., Auderset, A., Martínez-García, A., Modestou, S., & Meckler, A. N. (2020). Coupled Southern Ocean cooling and Antarctic ice sheet expansion during the middle Miocene. *Nature Geoscience*, *13*(9), 634–639. https://doi.org/10.1038/s41561-020-0623-0

Levitt, N. P., Eiler, J. M., Romanek, C. S., Beard, B. L., Xu, H., & Johnson, C. M. (2018). Near equilibrium ^{13}C–^{18}O bonding during inorganic calcite precipitation under chemo-stat conditions. *Geochemistry, Geophysics, Geosystems*, *19*(3), 901–920. https://doi.org/10.1002/2017gc007089

Lewis, P. D. E., & Wallace, D. W. R. (2006). MS Excel program developed for CO_2 system calculations. In *ORNL/CDIAC-105a*. Carbon Dioxide Information Analysis Center, Oak Ridge National Laboratory, US Department of Energy.

Loyd, S. J., Sample, J., Tripati, R. E., Defliese, W. F., Brooks, K., Hovland, M., et al. (2016). Methane seep carbonates yield clumped isotope signatures out of equilibrium with formation temperatures. *Nature Communications*, *7*(1), 12274. https://doi.org/10.1038/ncomms12274

McCrea, J. M. (1950). On the isotopic chemistry of carbonates and a paleotemperature scale. *The Journal of Chemical Physics*, *18*(6), 849–857. https://doi.org/10.1063/1.1747785

Millero, F. J. (1979). The thermodynamics of the carbonate system in seawater. *Geochimica et Cosmochimica Acta*, *43*(10), 1651–1661. https://doi.org/10.1016/0016-7037(79)90184-4

Mills, J. V., DePaolo, D. J., & Lammers, L. N. (2021). The influence of Ca:CO_3 stoichiometry on Ca isotope fractionation: Implications for process-based models of calcite growth. *Geochimica et Cosmochimica Acta*, *298*, 87–111. https://doi.org/10.1016/j.gca.2021.01.016

Petersen, S. V., Defliese, W. F., Saenger, C., Daeron, M., Huntington, K. W., John, C. M., et al. (2019). Effects of improved ^{17}O correction on interlaboratory agreement in clumped isotope calibrations, estimates of mineral-specific offsets, and temperature dependence of acid digestion fractionation. *Geochemistry, Geophysics, Geosystems*, *20*(7), 3495–3519. https://doi.org/10.1029/2018gc008127

Petersen, S. V., Dutton, A., & Lohmann, K. C. (2016). End-Cretaceous extinction in Antarctica linked to both Deccan volcanism and meteorite impact via climate change. *Nature Communications*, *7*(1), 12079. https://doi.org/10.1038/ncomms12079

Pokrovsky, O. S., Mielczarski, J. A., Barres, O., & Schott, J. (2000). Surface speciation models of calcite and dolomite/aqueous solution interfaces and their spectroscopic evaluation. *Langmuir*, *16*(6), 2677–2688. https://doi.org/10.1021/la980905e

Romanek, C. S., Grossman, E. L., & Morse, J. W. (1992). Carbon isotopic fractionation in synthetic aragonite and calcite: Effects of temperature and precipitation rate. *Geochimica et Cosmochimica Acta*, *56*(1), 419–430. https://doi.org/10.1016/0016-7037(92)90142-6

Sade, Z., Yam, R., Shemesh, A., & Halevy, I. (2020). Kinetic fractionation of carbon and oxygen isotopes during $BaCO_3$ precipitation. *Geochimica et Cosmochimica Acta*, *280*, 395–422. https://doi.org/10.1016/j.gca.2020.04.025

Saenger, C., Affek, H. P., Felis, T., Thiagarajan, N., Lough, J. M., & Holcomb, M. (2012). Carbonate clumped isotope variability in shallow water corals: Temperature dependence and growth-related vital effects. *Geochimica et Cosmochimica Acta*, *99*, 224–242. https://doi.org/10.1016/j.gca.2012.09.035

Saenger, C., Gabitov, R. I., Farmer, J., Watkins, J. M., & Stone, R. (2017). Linear correlations in bamboo coral $\delta^{13}C$ and $\delta^{18}O$ sampled by SIMS and micromill: Evaluating paleoceanographic potential and biomineralization mechanisms using $\delta^{11}B$ and Δ_{47} composition. *Chemical Geology*, *454*, 1–14. https://doi.org/10.1016/j.chemgeo.2017.02.014

Schauble, E. A., Ghosh, P., & Eiler, J. M. (2006). Preferential formation of ^{13}C–^{18}O bonds in carbonate minerals, estimated using first-principles lattice dynamics. *Geochimica et Cosmochimica Acta*, *70*(10), 2510–2529. https://doi.org/10.1016/j.gca.2006.02.011

Spooner, P. T., Guo, W., Robinson, L. F., Thiagarajan, N., Hendry, K. R., Rosenheim, B. E., & Leng, M. J. (2016). Clumped isotope composition of cold-water corals: A role for vital effects? *Geochimica et Cosmochimica Acta*, *179*, 123–141. https://doi.org/10.1016/j.gca.2016.01.023

Staudigel, P. T., & Swart, P. K. (2018). A kinetic difference between ^{12}C- and ^{13}C-bound oxygen exchange rates results in decoupled $\delta^{18}O$ and Δ_{47} values of equilibrating DIC solutions. *Geochemistry, Geophysics, Geosystems*, *19*(8), 2371–2383. https://doi.org/10.1029/2018gc007500

Tang, J., Dietzel, M., Fernandez, A., Tripati, A. K., & Rosenheim, B. E. (2014). Evaluation of kinetic effects on clumped isotope fractionation (Δ_{47}) during inorganic calcite precipitation. *Geochimica et Cosmochimica Acta*, *134*, 120–136. https://doi.org/10.1016/j.gca.2014.03.005

Thiagarajan, N., Adkins, J., & Eiler, J. (2011). Carbonate clumped isotope thermometry of deep-sea corals and implications for vital effects. *Geochimica et Cosmochimica Acta*, *75*(16), 4416–4425. https://doi.org/10.1016/j.gca.2011.05.004

Thiagarajan, N., Crémière, A., Blättler, C., Lepland, A., Kirsimäe, K., Higgins, J., et al. (2020). Stable and clumped isotope characterization of authigenic carbonates in methane cold seep environments. *Geochimica et Cosmochimica Acta*, *279*, 204–219. https://doi.org/10.1016/j.gca.2020.03.015

Tripati, A. K., Hill, P. S., Eagle, R. A., Mosenfelder, J. L., Tang, J., Schauble, E. A., et al. (2015). Beyond temperature: Clumped isotope signatures in dissolved inorganic carbon species and the influence of solution chemistry on carbonate mineral composition. *Geochimica et Cosmochimica Acta*, *166*, 344–371. https://doi.org/10.1016/j.gca.2015.06.021

Uchikawa, J., Chen, S., Eiler, J. M., Adkins, J. F., & Zeebe, R. E. (2021). Trajectory and timescale of oxygen and clumped isotope equilibration in the dissolved carbonate system under normal and enzymatically-catalyzed conditions at 25°C. *Geochimica et Cosmochimica Acta*, *314*, 313–333. https://doi.org/10.1016/j.gca.2021.08.014

Uchikawa, J., & Zeebe, R. E. (2012). The effect of carbonic anhydrase on the kinetics and equilibrium of the oxygen isotope exchange in the CO_2–H_2O system: Implications for $\delta^{18}O$ vital effects in biogenic carbonates. *Geochimica et Cosmochimica Acta*, *95*, 15–34. https://doi.org/10.1016/j.gca.2012.07.022

Uchikawa, J., & Zeebe, R. E. (2013). No discernible effect of Mg^{2+} ions on the equilibrium oxygen isotope fractionation in the CO_2–H_2O system. *Chemical Geology*, *343*, 1–11. https://doi.org/10.1016/j.chemgeo.2013.02.002

Vickers, M. L., Lengger, S. K., Bernasconi, S. M., Thibault, N., Schultz, B. P., Fernandez, A., et al. (2020). Cold spells in the Nordic Seas during the early Eocene Greenhouse. *Nature Communications*, *11*(1), 4713. https://doi.org/10.1038/s41467-020-18558-7

Wang, D. T., Gruen, D. S., Lollar, B. S., Hinrichs, K.-U., Stewart, L. C., Holden, J. F., et al. (2015). Nonequilibrium clumped isotope signals in microbial methane. *Science*, *348*(6233), 428–431. https://doi.org/10.1126/science.aaa4326

Watkins, J. M., & Hunt, J. D. (2015). A process-based model for non-equilibrium clumped isotope effects in carbonates. *Earth and Planetary Science Letters*, *432*, 152–165. https://doi.org/10.1016/j.epsl.2015.09.042

Watkins, J. M., Hunt, J. D., Ryerson, F. J., & DePaolo, D. J. (2014). The influence of temperature, pH, and growth rate on the $\delta^{18}O$ composition of inorganically precipitated calcite. *Earth and Planetary Science Letters*, *404*, 332–343. https://doi.org/10.1016/j.epsl.2014.07.036

Watkins, J. M., Nielsen, L. C., Ryerson, F. J., & DePaolo, D. J. (2013). The influence of kinetics on the oxygen isotope composition of calcium carbonate. *Earth and Planetary Science Letters*, *375*, 349–360. https://doi.org/10.1016/j.epsl.2013.05.054

Wolthers, M., Nehrke, G., Gustafsson, J. P., & Van Cappellen, P. (2012). Calcite growth kinetics: Modeling the effect of solution stoichiometry. *Geochimica et Cosmochimica Acta*, *77*, 121–134. https://doi.org/10.1016/j.gca.2011.11.003

Yumol, L. M., Uchikawa, J., & Zeebe, R. E. (2020). Kinetic isotope effects during CO_2 hydration: Experimental results for carbon and oxygen fractionation. *Geochimica et Cosmochimica Acta*, *279*, 189–203. https://doi.org/10.1016/j.gca.2020.03.041

Zeebe, R. E. (1999). An explanation of the effect of seawater carbonate concentration on foraminiferal oxygen isotopes. *Geochimica et Cosmochimica Acta*, *63*(13–14), 2001–2007. https://doi.org/10.1016/S0016-7037(99)00091-5

Zeebe, R. E., & Wolf-Gladrow, D. A. (2001). *CO_2 in seawater: Equilibrium, kinetics, isotopes*. Gulf Professional Publishing.

Zhang, J., Quay, P. D., & Wilbur, D. O. (1995). Carbon isotope fractionation during gas-water exchange and dissolution of CO_2. *Geochimica et Cosmochimica Acta*, *59*(1), 107–114. https://doi.org/10.1016/0016-7037(95)91550-D